

Quantum-beat imaging of the nuclear dynamics in D_2^+ : Dependence of bond softening and bond hardening on laser intensity, wavelength, and pulse duration

Maia Magrakvelidze,¹ Feng He,¹ Thomas Niederhausen,²
Igor V. Litvinyuk,¹ and Uwe Thumm¹

¹James R. Macdonald Laboratory, Kansas State University, Manhattan, Kansas 66506-2604, USA

²Departamento de Química, C-IX, Universidad Autónoma de Madrid, 28049 Madrid, Spain

Based on a quantum-mechanical model, we calculate the time evolution of an initial nuclear vibrational wave packet in D_2^+ generated by the rapid ionization of D_2 in an ultrashort pump-laser pulse. By Fourier transformation of the nuclear probability density with respect to the time delay between the pump pulse and the instant destructive Coulomb-explosion imaging of the wave packet at the high-intensity spike of an intense probe-laser pulse, we provide two-dimensional internuclear-distance-dependent power spectra that serve as a tool for visualizing and analyzing the nuclear dynamics in D_2^+ in an intermittent external laser field. The external field models the pedestal to the central ultrashort spike of a realistic probe pulse. Variation in the intensity, wavelength, and duration of this probe-pulse pedestal (i) allows us to identify the optimal laser parameters for the observation of field-induced bond softening and bond hardening in D_2^+ and (ii) suggests a scheme for quantitatively testing the validity of the ‘‘Floquet picture’’ that is commonly used for the interpretation of short-pulse laser-molecule interactions, despite its implicit ‘‘continuum wave’’ (*infinite* pulse length) assumption.

I. INTRODUCTION

The observation, analysis, and control of the time-dependent nuclear dynamics in small molecules have been made possible by recent advances in femtosecond (fs) laser technology, address our understanding of the basic concepts in quantum mechanics within atomic, molecular, and optical physics, and promise to significantly contribute towards reaching the ultimate goals of imaging and controlling complex chemical reactions with laser light [1–9]. Short and intense time-delayed laser pulses, which, for example, enable the time resolution of the nuclear motion in small diatomic molecules, are currently being employed in ‘‘pump-probe’’ experiments in many laboratories worldwide [10–19]. In such experiments on molecular targets, a neutral molecule is first ionized by a short pump-laser pulse. Short pulse lengths of only a few fs imply pump pulse bandwidths that are large compared to the vibrational level spacings. The pump pulse therefore *coherently* excites a superposition of stationary vibrational states of the molecular ion, resulting in a moving nuclear wave packet. The probability density of this wave packet can be imaged with the help of a second delayed ultrashort probe-laser pulse that rapidly (on the time scale of the nuclear motion) ionizes the molecular ion leading to its fragmentation by Coulomb explosion (CE) [20–22] and a measurable spectrum of fragment-kinetic-energy releases [10,13,23–25].

The dynamics of the nuclear wave packet can be reconstructed from the kinetic-energy release (KER) spectra obtained for a sequence of pump-probe delays τ [10,13]. This is shown schematically in Fig. 1 where a pump pulse singly ionizes a deuterium molecule. Within the Born-Oppenheimer (BO) approximation [26], the resulting nuclear wave packet evolves on the $1s\sigma_g^+$ ground-state potential curve in the deuterium molecular ion and is CE imaged by the time-delayed intense probe laser.

CE mapping [22,27] allows the measured KER spectra [8,10,11,13,23–25] to be compared with theoretical models for the nuclear probability densities [21,24,28–30]. In particular, for the simplest diatomic molecules, H_2^+ and its isotopologues, approximate nuclear probability densities can be provided by direct numerical solution of the time-dependent Schrödinger equation using wave-packet propagation techniques (and simplifying model assumptions, such as the representation of the nuclear and/or electronic motion in reduced dimensionality) [9,10,21,29,31]. For example, in recent experiments [10,11,13,24] the dephasing over a period of a few vibrational cycles of nuclear vibrational wave packets in D_2^+ and its subsequent revivals after many vibrational

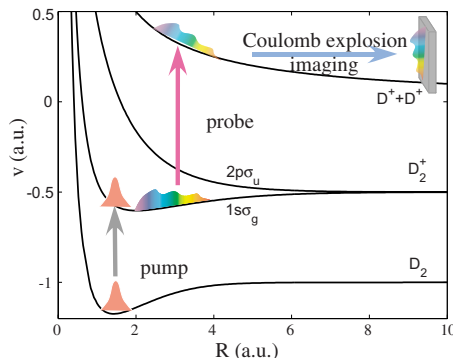


FIG. 1. (Color online) Schematic of the simulated KER measurement underlying the frequency-resolved investigation of the nuclear dynamics in D_2^+ discussed in this work. The pump-laser pulse launches a nuclear wave packet onto the D_2^+ $1s\sigma_g^+$ potential curve by ionizing D_2 and starts the molecular clock. After an adjustable time delay, an intense short probe pulse promotes the nuclear wave packet onto the $2D^+$ repulsive $1/R$ Coulomb-explosion curve and allows for the detection of the fragment-kinetic-energy distribution.

cycles were observed and confirmed earlier reduced-dimensionality model calculations [21]. This example shows that even without external forces, the field-free evolution of nuclear wave packets displays interesting purely quantum-mechanical phenomena. The evolution of the nuclear probability density is typically analyzed by recording the KER as a function τ which, after CE mapping, yields the nuclear probability density $\rho(R, \tau)$ [10,13]. Such graphs of $\rho(R, \tau)$ capture the nuclear dynamics in space (R) and time (τ) and allow the distinction of several pump-laser-induced phenomena, such as molecular fragmentation into different asymptotic dissociation channels and the coherent dephasing and revival [32] of bound vibrational wave packets in diatomic molecular ions [10,21,23,24,33,34].

An alternative and less explored method for investigating the nuclear dynamics in diatomic (and possibly in more complex) molecules is the time-series analysis of KER spectra. This method captures the nuclear dynamics in space and frequency and applies equally well to nuclear probability densities that are calculated or derived from measured KER spectra by CE mapping. It basically consists of first eliminating the strong static background $\rho_{\text{static}}(R)$ in the nuclear probability density and then Fourier transforming $\rho_{\text{dynamic}}(R, \tau) = \rho(R, \tau) - \rho_{\text{static}}(R)$ as a function of τ over a finite range $0 < \tau < T$ at fixed internuclear distances. This provides the R -dependent representation of the nuclear probability density $\tilde{\rho}_{\text{dynamic}}(R, f)$ as a function of the (quantum-beat) frequency f and the power spectrum $P(R, f; T) = |\tilde{\rho}_{\text{dynamic}}(R, f)|^2$. First applications of this time-series analysis method were recently published [8] and reveal features that are less obvious or not at all discernible in the more conventional “space-time” analysis of KER spectra [10,11,21,23,34]. In our previous investigations [30], we calculated $P(R, f; T)$ and examined the propagation of nuclear vibrational wave packets in D_2^+ in comparison with the first measured R -dependent quantum-beat spectra [8]. While these proof-of-principle studies illustrated the potential of the “space-frequency” (or quantum-beat) analysis of KER spectra for measuring (i) beat frequencies between stationary vibrational states in the electronic ground state of D_2^+ , (ii) the nodal structure of stationary vibrational states, (iii) the ground-state adiabatic electronic potential curve of the molecular ion, and (iv) laser-electric-field-dressed molecular potential curves, several questions remained open for further investigation.

In order to resolve the nuclear dynamics in small diatomic molecules in time, both pump and probe pulses need to be short on the time scale of the nuclear vibrational motion. For D_2^+ the vibrational period is about 20 fs and recent experiments succeed in resolving the nuclear motion with pulses with a nominal length of about 6–8 fs [8,10,24]. Such intense and ultrashort pulses typically have shapes that strongly deviate from the Gaussian or sin-squared profiles that are commonly used in model calculations. The shape of short laser pulses can be determined with the spectral phase interferometry for direct electric-field reconstruction (SPIDER) correlation technique [35]. For example, the SPIDER-analyzed intensity profile of the “6–7 fs” laser pulses used in the experiment of Feuerstein *et al.* [8] is characterized by a relatively long pedestal of approximately 100 fs length that underlies the central ultranarrow main peak of the pulse and

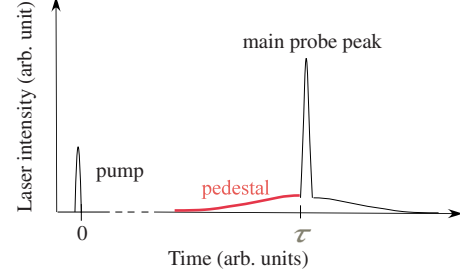


FIG. 2. (Color online) Schematic of the pump-probe sequence showing the main peak (black line) and pedestal (red line) of the probe pulse. In our simulations we use a Gaussian-shaped pedestal peak and assume instantaneous CE by ionization in main peak of the probe pulse

reaches about 5% of its peak intensity [23]. In the present work, in an attempt to model realistic pulses, we therefore include a pedestal in addition to the main spike of the pulse. In particular, the pedestal-to-probe pulse can strongly modify the nuclear dynamics immediately before it is probed by the sudden ionization of the molecular ion in the *main* probe peak (Fig. 2). In order to produce KER power spectra of sufficient resolution to distinguish adjacent vibrational quantum beats in D_2^+ , time delays need to be sampled over a time interval of about 1 ps [30]. Interestingly, this means that during a small fraction of the sampling time, a comparatively weak pedestal field can leave a pronounced effect on the observed KER spectra.

The pedestal pulses applied in this work will serve as prototypical intermittent laser fields, for which we analyze the effects on the evolution of nuclear wave packets. We thereby complement our previous work [8,30] on the quantum-beat analyzes of the nuclear motion in D_2^+ by discussing KER power spectra for an appropriate *range* of carrier frequencies, peak intensities, and pulse lengths of the intermittent laser field. This will allow us to (i) reveal the sensitivity of the laser-induced nuclear dynamics in response to the controlled change in the laser parameters frequency, intensity, and pulse length, (ii) assess the range of applicability of the Floquet interpretation [26,36] in *pulsed* laser-small molecule interactions, and (iii) restrict the range of laser parameters at which transient field-induced effects, such as bond softening (BS) [2,30,37–43] into different asymptotic Floquet channels and bond hardening (BH) [30,37,42–46], are most prominently displayed. Unless indicated otherwise, we assume atomic units (a.u.) throughout this work and designate the vibrational ground states of D_2 and D_2^+ with the index $\nu=0$ and excited states with $\nu \geq 1$.

II. THEORY

A. Two-state model for the nuclear wave-packet dynamics in D_2^+

We assume the neutral D_2 molecule to be singly ionized by an intense few-cycle pump pulse and approximate the quantum state of the resulting molecular ion as

$$\Phi(\vec{r}, R; t) = \frac{1}{\sqrt{2}} [\chi_g(R, t) \phi_g(R, \vec{r}) + \chi_u(R, t) \phi_u(R, \vec{r})], \quad (1)$$

where ϕ_g and ϕ_u are the D_2^+ electronic $1s\sigma_g$ and $2p\sigma_u$ states in BO approximation and \vec{r} is the position vector of the electron. In order to describe the bound and dissociating nuclear motions of the molecular ion in this two-electronic-state model, we project out the electronic states and obtain a set of coupled equations for the evolution of the gerade χ_g and ungerade χ_u nuclear wave-function components,

$$i \frac{\partial}{\partial t} \begin{pmatrix} \chi_g(R, t) \\ \chi_u(R, t) \end{pmatrix} = \begin{pmatrix} T_R + V_g(R) & D_{gu}(R)E(t-\tau) \\ D_{gu}(R)E(t-\tau) & T_R + V_u(R) \end{pmatrix} \times \begin{pmatrix} \chi_g(R, t) \\ \chi_u(R, t) \end{pmatrix}, \quad (2)$$

where $T_R = -\frac{1}{2\mu} \frac{\partial^2}{\partial R^2}$, $V_g(R)$ and $V_u(R)$ are the BO $1s\sigma_g$ and $2p\sigma_u$ potential curves, and μ is the reduced mass of the nuclei. The dipole coupling between gerade and ungerade states is designated by $D_{gu} = \langle \phi_g | r | \phi_u \rangle$ [40]. The linearly polarized laser field E is directed along the internuclear axis, and rotation of the molecular ion is not taken into consideration.

We numerically solve Eq. (2) using the Crank-Nicholson method [21,47] with time steps of $\Delta t = 1.0$ and spacial steps $\Delta R = 0.05$ with R covering the range between 0.05 and 30.0. We assume the initial state of the molecular ion to be bound,

$$\begin{aligned} \chi_g(R, 0) &= \sum_{\mu} a_{\mu} \chi_{\mu}(R), \\ \chi_u(R, 0) &= 0, \end{aligned} \quad (3)$$

such that it is specified by the set of (in general complex) amplitudes $\{a_{\mu}\}$ in the basis of stationary vibrational eigenstates $\{\chi_{\mu}\}$ of the electronic ground-state potential $V_g(R)$. We model the action of the pump pulse in sudden approximation with Franck-Condon (FC) factors $\{|a_{\mu}|^2\}$ and randomly set all phases to zero in order to obtain the set of *real* amplitudes $\{a_{\mu}\}$ for the bound initial wave packet. Numerically, we generate the real function $\chi_g(R, 0)$ by first calculating the ground state $|\chi_0\rangle$ of the neutral parent molecule by imaginary time propagation of a trial function on the ground-state BO potential curve of D_2 and subsequent projection on the D_2^+ vibrational states, $\{a_{\mu} = \langle \chi_{\mu} | \chi_0 \rangle\}$. In the absence of an external laser field, the two states in Eq. (2) are decoupled, and the nuclear wave function evolves as a bound nuclear wave packet on the $1s\sigma_g$ potential curve, undergoing characteristic cycles of dephasing and revival [21].

The time-delayed main peak of the probe pulse is assumed to instantaneously ionize the molecular ion and induce CE. In contrast, the probe-pulse pedestal is supposed to be weak enough to not contribute to the fragmentation of the molecular ion by CE. We do not need to include a pedestal to the pump pulse in our model (Fig. 2), as it would not change our numerical results presented below. For a given delay τ , our simulation of the evolution of the initial wave packet in D_2^+ thus starts at time $t=0$, immediately following the end of the (main) pump pulse, and ends at time $t=\tau$, immediately

preceding the main probe pulse, as indicated in Fig. 2. During the evolution, the pedestal (thick red line in Fig. 2)

$$E(t, \tau) = E_0 \sin[\omega(t - \tau)] \exp\left[-2 \ln 2 \left(\frac{t - \tau}{L}\right)^2\right] \quad (4)$$

is the only external field that couples χ_g and

$$\chi_u(R, t) = \int_0^{\infty} dE a_E e^{-iEt} \chi_E(R), \quad (5)$$

leading to the correlated motion of the nuclear wave packet on the $1s\sigma_g$ and $2p\sigma_u$ D_2^+ BO potential curves. The pedestal is specified by its amplitude E_0 , frequency ω , and the duration [full width at half maximum (FWHM) in the laser intensity] L . We will discuss the numerical results for a range of these parameters in Sec. III below. The dissociating part χ_u of the nuclear wave packet is written in terms of (continuum) eigenstates $\{|\chi_E\rangle\}$ in the $2p\sigma_u$ BO potential with (undetermined) coefficients $\{a_E\}$.

B. R-dependent quantum-beat power spectrum

For field-free propagation from $t=0$ to the probe time delay τ , the amplitudes $\{a_{\mu}\}$ in Eq. (3) remain time independent, and the nuclear probability density at time τ is

$$\begin{aligned} \rho(R, \tau) &= \int dr |\Phi(r, R, \tau)|^2 \\ &= |\chi_g(R, \tau)|^2 + |\chi_u(R, \tau)|^2 \\ &= \sum_{\mu} |a_{\mu}|^2 |\chi_{\mu}(R)|^2 + \sum_{\mu \neq \nu} a_{\mu}^* a_{\nu} e^{-i(E_{\nu} - E_{\mu})\tau} \chi_{\mu}^*(R) \chi_{\nu}(R). \end{aligned} \quad (6)$$

The diagonal terms in μ (third line) are time independent. By subtracting these incoherent static terms from Eq. (6), Fourier transformation of the coherent terms (fourth line) over the finite sampling time T , and taking the square of the result, we obtain the power spectrum

$$P(R, \omega; T) = \left| \sum_{\mu, \nu=0}^N a_{\mu}^* a_{\nu} \chi_{\mu}^*(R) \chi_{\nu}(R) \delta_T(\Delta\omega_{\mu, \nu} - \omega) \right|^2. \quad (7)$$

The complex-valued distribution

$$\delta_T(\Omega) \equiv \frac{1}{2\pi} \int_0^T dt e^{i\Omega t} = \frac{1}{\pi} e^{i\Omega T/2} \frac{\sin(\Omega T/2)}{\Omega} \quad (8)$$

is centered at the quantum-beat energies $\Delta\omega_{\mu, \nu} = \omega_{\nu} - \omega_{\mu}$. It is broadened due to the Fourier transformation over a *finite* time interval. In the limit of large sampling times, it becomes identical with the usual delta “function,” and the power spectrum $P(R, \omega; \infty)$ reproduces the quantum-beat spectrum at infinite resolution. In contrast, $T=3$ ps yields a finite-energy resolution of 2.7 meV, which allows for the distinction of quantum beats between virtually all populated vibrational states in the hydrogen molecular ion in $P(R, \omega; T)$. Further details on the properties and interpretation of $P(R, \omega; T)$ can be found in [30].

It is important to note that result (7) was derived under the assumption of *free* wave-packet propagation. It does not apply if external fields are present during the time propagation. However, it nevertheless constitutes a valuable guideline for the interpretation of external field effects in molecular power spectra if the external field acts during a time interval that is short compared to T . This condition is fulfilled in the recent experiment by Feuerstein *et al.* [8], where power spectra were measured with a sampling time of $T=3$ ps while the nuclear wave packet was exposed to an intermittent electric laser for less than 100 fs. All numerical examples in Sec. III below are calculated with $T=3$ ps and for pedestal pulse lengths of 200 fs or less. Equation (7) will therefore help in the interpretation of our numerical results. As will be shown below, this equation correctly describes the quantum-beat energy and several features that are related to the bound motion of the nuclei. It fails where strong-field effects become dominant, in particular, near the curve crossing points between field-dressed adiabatic molecular potential curves.

III. NUMERICAL RESULTS

In Floquet theory, the interaction of a molecule with a continuum wave (cw) laser field is represented in terms of adiabatic laser-dressed molecular potential curves [41,42,45,46], which we will also refer to as ‘‘Floquet adiabatic molecular potential curves’’ or simply ‘‘Floquet curves.’’ These Floquet curves are replicas of the field-free molecular potential curves that are shifted in energy due to the interaction with the laser field. The energy shifts amount to an increase or decrease in energy that is given by the net number of photons the molecule absorbs from or releases to the field. The absolute value of the Floquet energies is irrelevant and given relative to a laser field with a fixed macroscopic number of photons. Even though we consider short laser pulses for which the cw Floquet picture may not be applicable without restrictions, Floquet potential curves are a suitable reference for the description of laser-molecule interactions with laser pulses of finite duration.

As an example, Fig. 3 shows the Floquet adiabatic potential curves for D_2^+ in a 500 nm cw laser field for two different intensities, 5×10^{11} and 10^{13} W/cm², based on the two lowest field-free diabatic electronic potential curves of the molecular ion, $V_g(R)$ and $V_u(R)$ [48]. In the Floquet picture, field-free potential curves combine to form the field-dressed adiabatic potential curves. The Floquet curves are labeled as $1s\sigma_g - 2n\omega$ and $2p\sigma_u - (2n-1)\omega$, specifying the corresponding field-free potential curves and the net number of photons n that are released to the photon field. The dipole-allowed coupling between field-free potential curves of gerade and ungerade symmetries [26], due to the absorption or release of an odd number of photons, leads to characteristic ‘‘avoided’’ crossings between Floquet curves. The avoided crossings near internuclear distances of $R=4$ and $R=3$ originate in the exchange of one and three photons, respectively, between the molecular ion and cw laser field. The energetic gap between adjacent adiabatic field-dressed potential curves at the avoided crossing increases with increasing laser intensities.

Near the avoided crossing point and depending on the laser intensity, the more energetic field-dressed potential

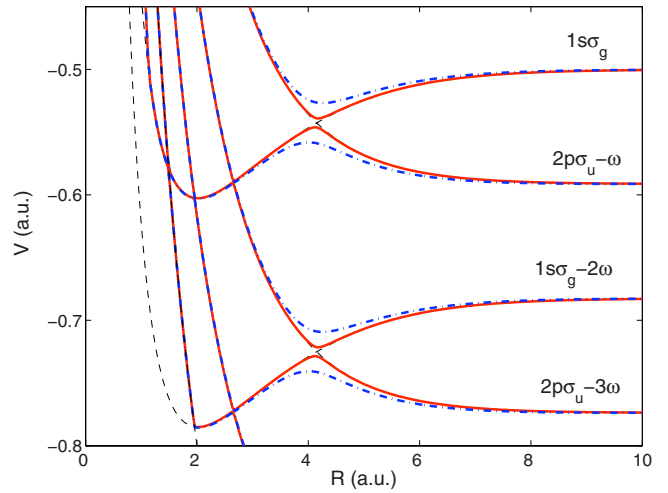


FIG. 3. (Color online) Laser-dressed adiabatic molecular potential curves for D_2^+ and a 500 nm cw laser field with an intensity of 5×10^{11} (solid red lines) and 10^{13} W/cm² (dashed-dotted blue lines). Thin black dashed lines show field-free BO potential curves.

curves may form a potential well, referred to as BH well, in which molecular probability density is trapped. Accordingly, the corresponding quantum states are called BH states. The BH well changes its shape with increasing laser intensity [37,42–46]. At higher intensities it becomes shallower and wider, and at sufficiently high intensities, loses the ability to bind BH states. In contrast to the BH well, the less energetic Floquet potential curve below the gap forms a barrier that may enable BS [2,37–39,41–43], i.e., dissociation of the molecule due either to classically allowed over-the-barrier escape or by tunneling.

The number of absorbed photons determines the KER. The dipole-allowed absorption of one or three photons leads to dissociation into the $1-\omega$ and $3-\omega$ dissociation channel, respectively. Dissociation by the effective absorption of an even number of photons can also occur, without violating the dipole selection rule, by proceeding over two avoided crossings. For example, exposed to sufficiently large laser intensities, D_2^+ can dissociate into the $2-\omega$ channel by first absorbing three and then releasing one photon.

Even though the numerical results presented in this work are in strong support of the interpretation of the laser-influenced nuclear motion in D_2^+ based on (time-independent) Floquet potential curves, we briefly mention an interesting alternative *dynamical* interpretation [49,50]. BH, which is also referred to as ‘‘vibrational trapping’’ or ‘‘dynamical dissociation quenching,’’ has been discussed by Châteauneuf *et al.* [49] in terms of the time-periodic potential curves $V_{\pm}(R,t)$ that are obtained by diagonalization of the field-free $1s\sigma_g$ and $2p\sigma_u$ BO potential curves subject to the time-dependent dipole coupling matrix elements $D_{gu}(R,t)$ at fixed t and R . The authors showed that the dynamical interplay between the time-dependent force associated with the upper $V_+(R,t)$ curve and the moving nuclear wave packet can lead to the efficient quenching of the laser-induced dissociation. This is in agreement with the classical interpretation of the nuclear motion, receiving an inward directed restoring force if the moving potential barrier included in

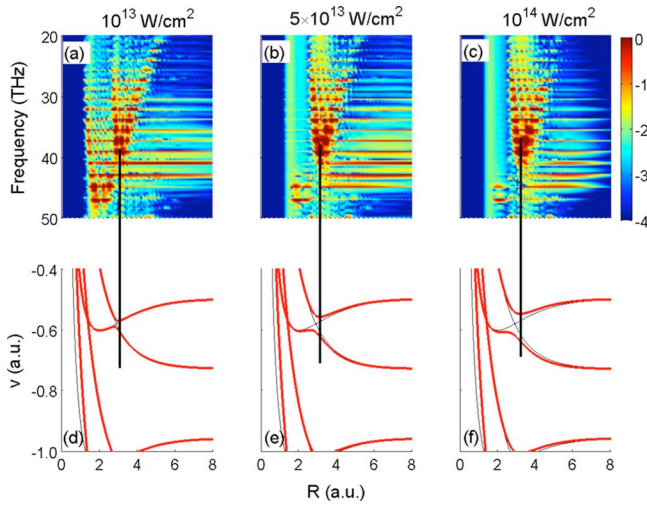


FIG. 4. (Color online) Pedestal intensity dependence for an initial FC vibrational wave packet in D_2^+ that propagates through 200 nm pedestal laser pulses with intensities of $0.1 \times$ [graphs (a) and (d)], $0.5 \times$ [graphs (b) and (e)], and 1×10^{14} W/cm^2 [graphs (c) and (f)]. [(a)–(c)] Power spectra (logarithmic color scale) as a function of the quantum-beat frequency f and the internuclear distance R . [(d)–(f)] Field-dressed adiabatic potential curves (thick red lines) for the same intensities. Thin black lines show field-free potential curves.

$V_+(R, t)$ is appropriately synchronized with the nuclear motion. This dynamical interpretation of BH was experimentally confirmed for the nuclear motion in H_2^+ and D_2^+ in a 70 fs $1.6 \mu m$ laser pulse that was modulated on the time scale of the nuclear vibrational motion (10 fs) [50]. The modulation was obtained by the coherent superposition of two laser pulses and provided an adjustable pulse envelope that controls the motion of the vibrational wave packet.

In Secs. III A–III C, we will discuss the bound and dissociating nuclear motion of D_2^+ in a laser pulse by examining how power spectra are affected by the laser pedestal parameters intensity, frequency, and duration. Even though all simulations were carried out for (pedestal) laser pulses with a finite pulse length, we will show that the terminology developed based on the Floquet picture is appropriate. For example, even though stable BH states can only exist in cw laser fields, we find evidence for transient BH states in laser pulses over a large range of pulse lengths.

A. Intensity dependence

R -dependent power spectra $P(R, \omega; T)$ for D_2^+ propagating through 200 nm 20 fs (FWHM) Gaussian pedestal laser pulses with different peak intensities are shown in the upper panels of Fig. 4. The corresponding Floquet field-dressed potential curves are displayed in red in the lower panels. The field-free adiabatic molecular potential curves are also included in the lower panels as thin black lines. As for all other numerical results shown further below, the molecular ion is assumed to be produced by the rapid ionization of D_2 and is characterized by a FC distribution of stationary vibrational states, as described above. The three columns show results

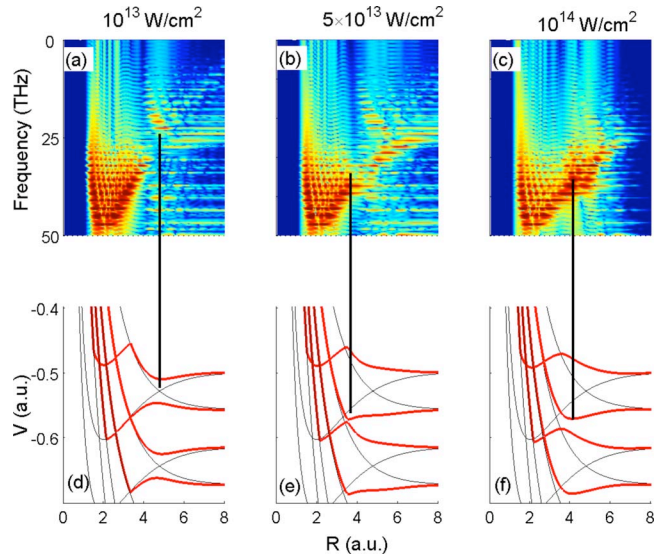


FIG. 5. (Color online) Same as Fig. 4 for 800 nm pedestal laser pulses.

for pedestal intensities of 10^{13} (left), 5×10^{13} (middle), and 10^{14} W/cm^2 (right column).

For the frequency and R range shown in Fig. 4, the R dependence in the power spectra (7) reflects the nodal structure of the product of the probability densities $|a_\mu|^2$ and $|a_\nu|^2$ of the two adjacent stationary vibrational states $|\chi_\mu\rangle$ and $|\chi_\nu\rangle$ that beat against each other with the frequency $f = \Delta\omega_{\mu,\nu}/(2\pi)$ [30]. The thin black vertical lines facilitate the association of minima of the $1-\omega$ BH wells in the power spectra (upper row of graphs in Fig. 4) with BH wells in the Floquet potential curves (lower row). For the displayed intensities, the power spectra show a significant amount of nuclear probability density that is intermittently trapped in the $1-\omega$ BH well.

The nuclear probability density in the $1-\omega$ BH well increases with intensity at the expense of probability that is associated with the bound motion of the molecular ions in field-dressed $1s\sigma_g$ potential curve. The power spectra confirm the intuitive expectation that dissociation across the $1-\omega$ BS barrier, either by classical over-the-barrier motion of the two nuclei or by tunneling, (i) increases with increasing peak intensity and (ii) progresses by first depleting the highest vibrational state components of the nuclear wave packet with vibrational quantum numbers $\nu \geq 4$ (at quantum-beat frequencies near 40 THz) (left column in Fig. 4) to the lowest vibrational components of the initial FC distribution (right column).

B. Wavelength dependence

For shorter wavelengths and otherwise identical laser parameters, the character of the power spectra changes. In comparison with the 200 nm results in Fig. 4, the power spectra calculated for 800 nm in Fig. 5 indicate that the nuclear motion in D_2^+ sensitively depends on the carrier wavelength. To a large extent, this change can be understood within the Floquet picture. As the photon energy decreases, the spacing

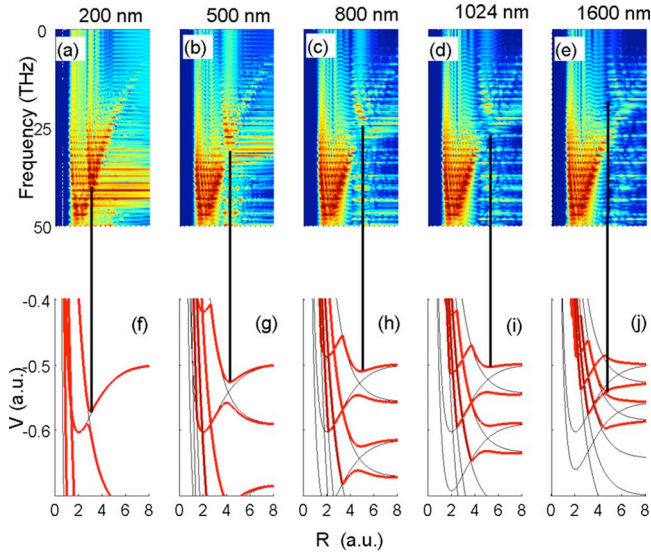


FIG. 6. (Color online) Laser wavelength dependence for an initial FC vibrational wave packet in D_2^+ that propagates through 10^{13} W/cm² peak intensity pedestal laser pulses with wavelengths of 200 [graphs (a) and (f)], 500 [graphs (b) and (g)], 800 [graphs (c) and (h)], 1024 [graphs (d) and (i)], and 1600 nm [graphs (e) and (j)]. [(a)–(e)] Power spectra (same logarithmic color scale as in Fig. 4) as a function of the quantum-beat frequency f and the internuclear distance R . [(f)–(j)] Field-dressed adiabatic potential curves (thick red lines) for the same intensities. Thin black lines show field-free potential curves.

in energy between Floquet potential curves decreases. This decrease increases the significance of couplings between more than two curves, which, in turn, may result in the overlap of ($1-\omega$ with $3-\omega$) BH wells and their bond-prohibiting flattening. At 800 nm and 10^{13} W/cm² peak intensity (left column in Fig. 5), the power spectrum shows only weak evidence for the temporary trapping of nuclear probability density in the $1-\omega$ BH well that is centered near $R=5$. The molecular ion remains most likely bound in the electronic ground state. At the higher intensities (middle and right columns), dissociation via BS becomes increasingly important but cannot be as clearly assigned to the $1-\omega$ BS barrier as for the case of 200 nm wavelength.

At 800 nm and 5×10^{13} W/cm² (middle column in Fig. 5), the $1-\omega$ BH well has disappeared in the Floquet potential curve (graph e) and BH is mostly confined to the $3-\omega$ BH well centered at smaller distances near $R=3.5$ in the power spectrum. The same applies to the highest shown intensity (10^{14} W/cm², right column) where dissociation via $1-\omega$, and to a lesser extent, $3-\omega$ BS, strongly decreases the molecular ion's chance for survival in the bound electronic ground state. Note that graph (b) also shows weak evidence for BH states in the $1-\omega$ well near $R=5$ due to temporary vibrational trapping during the increasing laser intensity of the pedestal, although graph (e) would prohibit such states.

A more systematic study of the wavelength dependence of BS and BH is shown in Fig. 6 for power spectra (upper row) and Floquet potential curves at a fixed intensity of 10^{13} W/cm². Since the crossing point in the field-free potential curves (thin black lines in the lower panels) changes

with the photon energy, we expect that the laser wavelength will affect BS and BH. The power spectra in graphs (a)–(e) show that dissociation by BS decreases with increasing wavelength, while the $1-\omega$ BH well moves to larger internuclear distances. For 200 nm wavelength graphs (a) and (f) show a very prominent $1-\omega$ BH well due to the strong coupling between the $1s\sigma_g$ and $2p\sigma_u$ electronic states. For this wavelength, all vibrational eigenstates in the initial FC distribution above $\nu=2$ are being depleted by BS, while the deep BH well traps even the highest initially occupied vibrational states.

For 500 nm [Figs. 6(b) and 6(g)] the $1-\omega$ BH well remains populated but receives less probability density than for the case of 200 nm, while the nuclear motion is more likely to remain bound in the electronic ground state. This trend continues for 800, 1024, and 1600 nm (three right columns in Fig. 6) to the point that BH in the $1-\omega$ well disappears at 1600 nm. This also follows from the comparison of Figs. 4(c) and 5(c) above. As the wavelength increases, BS through and over the $3-\omega$ well becomes energetically possible for an increasing number of stationary vibrational states of the nuclear wave packet. However, as the simulated power spectra show, the peak intensity of 10^{13} W/cm² is too low for three-photon processes to become relevant. Therefore, $3-\omega$ BS and BH are not clearly noticeable in Fig. 6.

In the left four columns of Fig. 6, the positions of the $1-\omega$ BH well agree in power spectra and Floquet potential curves. At 1600 nm, however, according to the Floquet picture the $1-\omega$ BH has disappeared and BH is expected to happen near the $3-\omega$ crossing point [Fig. 6(j)]. This prediction of the cw Floquet picture is not fully confirmed in the power spectrum in Fig. 6(e) that shows very weak evidence of $1-\omega$ BH states centered near $R=7$ and no apparent traces of $3-\omega$ BS or BH. This mismatch is related to the fact that the Floquet picture assumes infinite pulse lengths, while at 1600 nm the power spectrum simulates the propagation of the nuclear wave packet across a pedestal pulse with a length of $L=20$ fs (FWHM), corresponding to the illumination of the wave packet by the pedestal laser pulse over just two optical cycles and with a rapidly changing envelope. We therefore interpret this discrepancy as due to both the onset of the breakdown of the Floquet picture for short pulses, and more importantly, an *effective* laser intensity in the power spectra that is much smaller than the peak intensity for which the Floquet curves were calculated.

C. Pulse-length dependence

The combined effect on the power spectra of changing pulse duration and wavelength is shown in Fig. 7. The panels in this figure are ordered with pedestal wavelengths increasing from 200 (top) to 1600 nm (bottom). The pedestal length increases from $L=50$ (FWHM, left) to 200 fs (right). For each wavelength (each row), the BH probability decreases with increasing pulse length. Even though one might expect longer pedestal pulses to enable more pronounced BH due to longer trapping times, our simulations show the opposite trend which we assign to the dominant influence of the pulse energy. Longer pedestals transfer more energy to the mol-

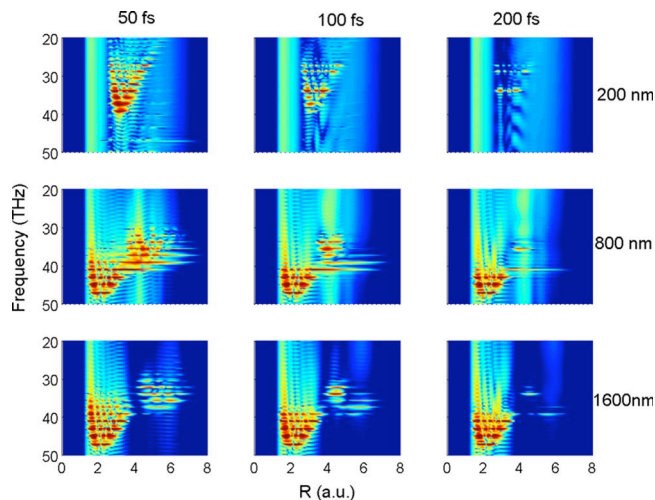


FIG. 7. (Color online) Power spectra (same logarithmic color scale as in Fig. 4) as a function of the quantum-beat frequency f and the internuclear distance R . Propagation of an initial FC wave packet for probe-pulse pedestals with a peak intensity of 10^{14} W/cm², wavelengths of 200, 800, and 1600 nm, and pulse lengths (FWHM) of 50, 100, and 200 fs. The wave packet is sampled at the center of the probe.

ecule. This favors both dissociation by BS directly out at the electronic ground state (leaving less probability to be potentially trapped in a BH well) and the decay of BH states by nonadiabatic couplings to dissociative potential curves that are neglected in the BO approximation [26].

At shorter wavelengths, the same pedestal pulse envelope includes more optical cycles. Thus, the power spectra in Fig. 7 with the shortest wavelength and longest pulse duration are most amenable to their interpretation within the Floquet picture. However, this trend is somewhat difficult to follow over a large range of pulse lengths, since, for high pulse durations (high pulse energies), BS can dominate to the point that all bound states become depleted. This is illustrated in the top-right corner of Fig. 7. For a wavelength of 200 nm (top row), BS dissociation is rapidly depleting the electronic ground

state and leaves a noticeable population in the $1-\omega$ BH well only for the lowest shown pulse energy ($L=50$ fs). At 800 and 1600 nm, in contrast, the electronic ground state remains populated at all displayed pulse lengths but, as expected, gets increasingly depleted with increasing pulse length by BS over and through the $1-\omega$ BS barrier. The comparison of all panels in Fig. 7 suggests that BH is most pronounced at the shortest wavelengths and for the shortest pedestals. The comparison with Fig. 4 above shows that BH at short wavelengths is robust over a large range in peak intensities.

IV. CONCLUSIONS

Based on simulated R -dependent quantum-beat power spectra, we imaged the nuclear dynamics in D_2^+ molecular ions that are exposed to short laser pulses with different peak intensities, wavelengths, and pedestal lengths. We analyzed these spectra in terms of field-dressed Floquet potential curves with emphasis on dissociation by BS and transient binding of the nuclear motion by BH. Except for the longest wavelengths used in our simulations (1600 nm), we confirmed the Floquet picture as appropriate for characterizing the main features of the nuclear dynamics in few-cycle laser pulses despite its inherent cw assumption. Our simulations suggest that pulses with a wavelength between 200 to 300 nm, a peak intensity of about 10^{14} W/cm², and a duration of less than 50 fs (FWHM) are well suited for the observation of transient vibration trapping of the molecular motion in the $1-\omega$ BH well. At wavelengths of 1600 nm, we found that dissociation proceeds via both $1-\omega$ and $3-\omega$ BS. For the same wavelength, our simulations indicate transient trapping in the $3-\omega$ BH well. To the best of our knowledge, existing technology [5,8] allows for the detailed experimental test of our findings.

ACKNOWLEDGMENTS

This work was supported by the NSF and the Division of Chemical Sciences, Office of Basic Energy Sciences, Office of Science, U.S. DOE.

-
- [1] A. H. Zewail, *J. Phys. Chem. A* **104**, 5660 (2000).
 [2] J. H. Posthumus, *Rep. Prog. Phys.* **67**, 623 (2004).
 [3] M. Dantus and V. V. Lozovoy, *Chem. Rev. (Washington, D.C.)* **104**, 1813 (2004).
 [4] T. Brixner, T. Pfeifer, G. Gerber, M. Wollenhaupt, and T. Baumert, in *Femtosecond Laser Spectroscopy*, edited by P. Hannaford (Springer, New York, 2005), Chap. 9.
 [5] I. V. Hertel and W. Radloff, *Rep. Prog. Phys.* **69**, 1897 (2006).
 [6] M. F. Kling, Ch. Siedschlag, A. J. Verhoef, J. I. Khan, M. Schultze, Th. Uphues, Y. Ni, M. Uiberacker, M. Drescher, F. Krausz, and M. J. J. Vrakking, *Science* **312**, 246 (2006).
 [7] A. Staudte, D. Pavicic, S. Chelkowski, D. Zeidler, M. Meckel, H. Niiikura, M. Schöffler, S. Schössler, B. Ulrich, P. P. Rajeev, Th. Weber, T. Jahnke, D. M. Villeneuve, A. D. Bandrauk, C. L. Cocke, P. B. Corkum, and R. Dörner, *Phys. Rev. Lett.* **98**, 073003 (2007).
 [8] B. Feuerstein, Th. Ergler, A. Rudenko, K. Zrost, C. D. Schröter, R. Moshhammer, J. Ullrich, T. Niederhausen, and U. Thumm, *Phys. Rev. Lett.* **99**, 153002 (2007).
 [9] F. He, A. Becker, and U. Thumm, *Phys. Rev. Lett.* **101**, 213002 (2008).
 [10] A. S. Alnaser, B. Ulrich, X. M. Tong, I. V. Litvinyuk, C. M. Maharjan, P. Ranitovic, T. Osipov, R. Ali, S. Ghimire, Z. Chang, C. D. Lin, and C. L. Cocke, *Phys. Rev. A* **72**, 030702(R) (2005).
 [11] F. Légaré, Kevin F. Lee, I. V. Litvinyuk, P. W. Dooley, A. D. Bandrauk, D. M. Villeneuve, and P. B. Corkum, *Phys. Rev. A* **72**, 052717 (2005).
 [12] A. Bhattacharjee and K. R. Dastidar, *Phys. Rev. A* **72**, 023419 (2005).

- [13] T. Ergler, A. Rudenko, B. Feuerstein, K. Zrost, C. D. Schröter, R. Moshhammer, and J. Ullrich, *Phys. Rev. Lett.* **97**, 193001 (2006).
- [14] S. Baker, J. S. Robinson, C. A. Haworth, H. Teng, R. A. Smith, C. C. Chirila, M. Lein, J. W. G. Tisch, and J. P. Marangos, *Science* **312**, 424 (2006).
- [15] G. Sansone, E. Benedetti, F. Calegari, C. Vozzi, L. Avaldi, R. Flammini, L. Poletto, P. Villoresi, C. Altucci, R. Velotta, S. Stagira, S. De Silvestri, and M. Nisoli, *Science* **314**, 443 (2006).
- [16] P. B. Corkum and F. Krausz, *Nat. Phys.* **3**, 381 (2007).
- [17] D. S. Murphy, J. McKenna, C. R. Calvert, W. A. Bryan, E. M. L. English, J. Wood, I. C. E. Turcu, W. R. Newell, I. D. Williams, and J. F. McCann, *J. Phys. B* **40**, S359 (2007).
- [18] P. Johnsson, J. Mauritsson, T. Remetter, A. L'Huillier, and K. J. Schafer, *Phys. Rev. Lett.* **99**, 233001 (2007).
- [19] L. Miaja-Avila, G. Saathoff, S. Mathias, J. Yin, C. La-ovorakiat, M. Bauer, M. Aeschlimann, M. M. Murnane, and H. C. Kapteyn, *Phys. Rev. Lett.* **101**, 046101 (2008).
- [20] S. Chelkowski and A. D. Bandrauk, *Phys. Rev. A* **65**, 023403 (2002).
- [21] B. Feuerstein and U. Thumm, *Phys. Rev. A* **67**, 043405 (2003); **67**, 063408 (2003).
- [22] S. Chelkowski, A. D. Bandrauk, A. Staudte, and P. B. Corkum, *Phys. Rev. A* **76**, 013405 (2007).
- [23] A. Rudenko, T. Ergler, B. Feuerstein, K. Zrost, C. D. Schröter, R. Moshhammer, and J. Ullrich, *Chem. Phys.* **329**, 193 (2006).
- [24] H. Niikura, D. M. Villeneuve, and P. B. Corkum, *Phys. Rev. A* **73**, 021402(R) (2006).
- [25] F. Martín, J. Fernández, T. Havermeier, L. Foucar, Th. Weber, K. Kreidi, M. Schöffler, L. Schmidt, T. Jahnke, O. Jagutzki, A. Czasch, E. P. Benis, T. Osipov, A. L. Landers, A. Belkacem, M. H. Prior, H. Schmidt-Böcking, C. L. Cocke, and R. Dörner, *Science* **315**, 629 (2007).
- [26] B. H. Bransden and C. J. Joachain, *Physics of Atoms and Molecules*, 2nd ed. (Prentice-Hall, London, 2003).
- [27] B. Feuerstein and U. Thumm, *J. Phys. B* **36**, 707 (2003).
- [28] H. Niikura, D. M. Villeneuve, and P. B. Corkum, *Phys. Rev. Lett.* **92**, 133002 (2004).
- [29] D. S. Murphy, J. McKenna, C. R. Calvert, I. D. Williams, and J. F. McCann, *New J. Phys.* **9**, 260 (2007).
- [30] U. Thumm, T. Niederhausen, and B. Feuerstein, *Phys. Rev. A* **77**, 063401 (2008).
- [31] S. Chelkowski, P. B. Corkum, and A. D. Bandrauk, *Phys. Rev. Lett.* **82**, 3416 (1999).
- [32] R. W. Robinett, *Phys. Rep.* **392**, 1 (2004).
- [33] I. A. Bocharova, H. Mashiko, M. Magrakvelidze, D. Ray, P. Ranitovic, C. L. Cocke, and I. V. Litvinyuk, *Phys. Rev. A* **77**, 053407 (2008).
- [34] J. McKenna, W. A. Bryan, C. R. Calvert, E. M. L. English, J. Wood, D. D. Murphy, I. C. E. Turcu, J. M. Smith, K. G. Ertel, O. Chekhlov, E. J. Divall, J. F. McCann, W. R. Newell, and I. D. Williams, *J. Mod. Opt.* **54**, 1127 (2007).
- [35] C. Iaconis and A. Walmsley, *Opt. Lett.* **23**, 792 (1998).
- [36] S. R. Barone, M. A. Narcowich, and F. J. Narcowich, *Phys. Rev. A* **15**, 1109 (1977).
- [37] A. D. Bandrauk and M. L. Sink, *J. Chem. Phys.* **74**, 1110 (1981).
- [38] A. Giusti-Suzor, X. He, O. Atabek, and F. H. Mies, *Phys. Rev. Lett.* **64**, 515 (1990).
- [39] P. H. Bucksbaum, A. Zavriyev, H. G. Muller, and D. W. Schumacher, *Phys. Rev. Lett.* **64**, 1883 (1990).
- [40] K. C. Kulander, F. H. Mies, and K. J. Schafer, *Phys. Rev. A* **53**, 2562 (1996).
- [41] I. D. Williams, P. McKenna, B. Srigengan, I. M. G. Johnston, W. A. Bryan, J. H. Sanderson, A. El-Zein, T. R. J. Goodworth, W. R. Newell, P. F. Taday, and A. J. Langley, *J. Phys. B* **33**, 2743 (2000).
- [42] K. Sändig, H. Figger, and T. W. Hänsch, *Phys. Rev. Lett.* **85**, 4876 (2000).
- [43] H. Abou-Rachid, T. T. Nguyen-Dang, and O. Atabek, *J. Chem. Phys.* **114**, 2197 (2001).
- [44] L. J. Frasinski, J. H. Posthumus, J. Plumridge, K. Codling, P. F. Taday, and A. J. Langley, *Phys. Rev. Lett.* **83**, 3625 (1999).
- [45] L. J. Frasinski, J. Plumridge, J. H. Posthumus, K. Codling, P. F. Taday, E. J. Divall, and A. J. Langley, *Phys. Rev. Lett.* **86**, 2541 (2001).
- [46] A. Giusti-Suzor and F. H. Mies, *Phys. Rev. Lett.* **68**, 3869 (1992).
- [47] W. H. Press, S. A. Teukolsky, W. T. Vetterling, and B. P. Flannery, *Numerical Recipes* (Cambridge University Press, Cambridge, England, 1992).
- [48] D. R. Bates, K. Ledsham, and A. L. Stewart, *Philos. Trans. R. Soc. London, Ser. A* **246**, 215 (1953).
- [49] F. Châteauneuf, T. T. Nguyen-Dang, N. Quellet, and O. Atabek, *J. Chem. Phys.* **108**, 3974 (1998).
- [50] H. Niikura, P. B. Corkum, and D. M. Villeneuve, *Phys. Rev. Lett.* **90**, 203601 (2003).

